Bacteria-mediated delivery of nanoparticles and cargo into cells

DEMIR AKIN[1,2,3]*, JENNIFER STURGIS[2,4], KATHY RAGHEB[2,4], DEBBY SHERMAN[5], KRISTIN BURKHOLDER[6], J. PAUL ROBINSON[2,3,4], ARUN K. BHUNIA[6], SULMA MOHAMMED[7] AND RASHID BASHIR[1,2,3,8]*

[1]Birck Nanotechnology Center, Purdue University, 1205 W State Street, West Lafayette, Indiana 47907, USA
[2]Bindley Biosciences Center, Purdue University, West Lafayette, Indiana 47907, USA
[3]Weldon School of Biomedical Engineering, Purdue University, 206 S Intramural Drive, West Lafayette, Indiana 47907, USA
[4]Department of Basic Medical Sciences, Purdue University, West Lafayette, Indiana 47907, USA
[5]Department of Biology, Purdue University, West Lafayette, Indiana 47907, USA
[6]Molecular Food Microbiology Laboratory, Department of Food Science, 745 Agriculture Mall Drive, West Lafayette, Indiana 47907, USA
[7]Department of Comparative Pathobiology, 725 Harrison Street, West Lafayette, Indiana 47907, USA
[8]School of Electrical and Computer Engineering, Purdue University, West Lafayette, Indiana 47907, USA
*e-mail: akin@purdue.edu; bashir@purdue.edu

Nanoparticles and bacteria can be used, independently, to deliver genes and proteins into mammalian cells for monitoring or altering gene expression and protein production. Here, we show the simultaneous use of nanoparticles and bacteria to deliver DNA-based model drug molecules *in vivo* and *in vitro*. In our approach, cargo (in this case, a fluorescent or a bioluminescent gene) is loaded onto the nanoparticles, which are carried on the bacteria surface. When incubated with cells, the cargo-carrying bacteria ('microbots') were internalized by the cells, and the genes released from the nanoparticles were expressed in the cells. Mice injected with microbots also successfully expressed the genes as seen by the luminescence in different organs. This new approach may be used to deliver different types of cargo into live animals and a variety of cells in culture without the need for complicated genetic manipulations.

One of the most significant challenges facing the treatment of diseases is early intervention to deliver specific therapeutic cargo efficiently into cells to alter gene expression and subsequent protein production. Recent advances in nanotechnology have been used to deliver such cargoes into single cells through the use of nanoparticles for imaging[1–3], diagnostics[4,5] and therapeutics[6–8]. Although significant advances have been made, many difficulties remain in delivering the nanoparticles to the tumour sites, mainly because of the physical barriers encountered in solid tumours, such as malformed blood supplies, elevated interstitial pressure, and large transport distances in the tumour interstitium[9,10].

Bacteria have been used as a non-viral means to transfer plasmid DNA into mammalian cells through a process called 'bactofection' (reviewed in ref. 11). Several intracellular bacteria, including *Listeria monocytogenes*, which is responsible for food-borne infections in humans and animals[12], can penetrate mammalian cells that are normally non-phagocytic. These bacteria need specific surface molecules that interact with host-cell receptors for this invasion step[13–15] once inside the cells, the bacteria carriers are disrupted—by treatment with antibiotics—and the DNA is released. *L. monocytogenes*-based bactofection systems have shown efficient transfer of genetic material inside the cells[16,17]. Other earlier reports include use of attenuated (reduced infectivity) bacteria such as *Shigella*[18] and *Salmonella typhimurium*[19,20] for the delivery of DNA-based vaccines. Bacteria

themselves have additional advantages as delivery systems. For example, attenuated strains of *Escherichia coli*, *S. typhimurium*, *Vibrio cholerae* and *L. monocytogenes* have been shown to be capable of multiplying selectively in tumours[21], and in the case of *Clostridium* and *Bifidobacterium* spp., they even inhibit tumour growth[20,22]. Some of the unique properties of attenuated Listeria strains make them an ideal non-viral gene delivery vehicle[23–25]. It should also be noted that antibiotics can control bacterial replication in the body or activate gene-based therapeutic molecules, as in the case with tetracycline-regulated control of gene expression[26].

Here, we report a novel technique for delivery of nanoparticles into cells, which takes advantage of the invasive properties of bacteria. The gene or cargo is not carried inside the bacteria, but rather remains on the surface conjugated to nanoparticles. Hence, our approach does not require bacterial disruption for delivery, or any genetic engineering of the bacteria for different cargo. Although more than one gene can be delivered by means of bactofection, many more copies of a target cargo can be carried with one bacterium using the method described here. We also show that nucleic acid-based model drugs (plasmid DNAs coding for green fluorescence protein (GFP), luciferase and secreted alkaline phosphatase (SEAP)) loaded on the nanoparticles can be released from the carriers and eventually find their way into the nucleus, with subsequent transcription and translation of their respective proteins, for both *in vitro* and

1
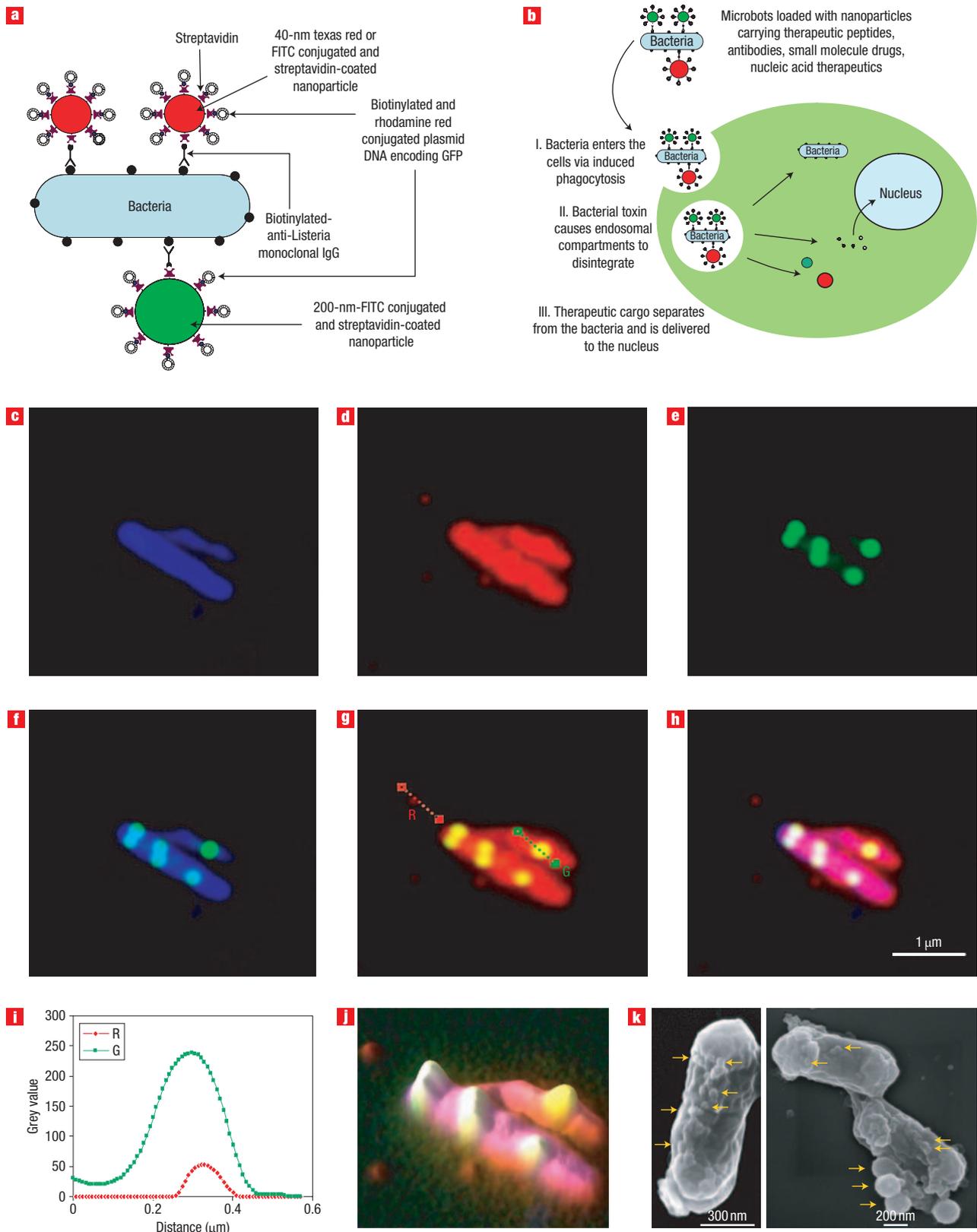
Figure 1 Bacteria-mediated delivery of nanoparticles and cargo. a, Docking of bacteria with functionalized multiple-sized nanoparticles through biotinylated antibodies and surface–antigen interactions (microbots). Streptavidin-coated nanoparticles can carry biotinylated cargo. **b**, Delivery of intervention agents using microbots. **c–k**, Assembled microbots with their cargos: bacteria (blue) (**c**), streptavidin-coated 40-nm fluorescent-red nanoparticles (**d**), neutravidin-coated 200-nm fluorescent-green nanoparticles (**e**). **f–h**, Overlays of images **c** and **e** (**f**), images **d** and **e** (**g**), and images **c–e** (**h**). **i**, Profiles of lines G and R from **g**. **j**, Simulated height image. **k**, SEM images of microbots (arrows show nanoparticles).

in vivo conditions. Such bacteria, which we call 'microbots', can potentially be used to carry proteins, small molecules and even synthetic objects like sensors and therapeutic moieties into different types of cells.

MICROBOTS DELIVER NANOPARTICLES AND DNA INTO CELLS

Our approach for preparing the microbots uses biotinylated monoclonal antibody C11E9[27,28] against a surface protein, N-acetylmuramidase[29], on *L. monocytogenes* bacteria to attach streptavidin-coated polystyrene nanoparticles onto the bacterial surface. Biotinylated GFP plasmid was then attached to the remaining streptavidin sites on the nanoparticles (Fig. 1a) (see Methods). This generalized approach can be used to attach particles of various sizes or different entities onto Listeria to be delivered into eukaryotic cells (Fig. 1b). We characterized the attachment of the particles on individual bacteria with fluorescence imaging (Fig. 1c−j) and scanning electron microscopy (SEM) (Fig. 1k). Fluorescence images of biotinylated antibody-covered Listeria incubated with streptavidin-coated 40 nm (red) and 200 nm (green) nanoparticles clearly show that the bacterium, which was stained blue, is co-localizing with the 40-nm Texas red-labelled nanoparticles and 200-nm FITC green-labelled nanoparticles (Fig. 1c−j), thus proving that the same bacteria can carry different size particles.

When fluorescently labelled bacteria were incubated with KB (human nasopharyngeal carcinoma) cells for up to 3 h at 37 °C, bacteria entered the cytosol of the cells and resulted in significant bacterial replication in the cells (see Supplementary Information, Fig. S1 and video). Incubation of the cells with the biotinylated anti-*L. monocytogenes* monoclonal antibody did not neutralize the infectivity of the microbots (see Supplementary Information, Table S1). We next attempted to deliver nanoparticles docked on the bacterial cell surface as described in the Methods. The 200-nm particles on their own were not internalized by the cells within the 3 h period, but rather were associated with the cell surface (Fig. 2a), as also verified by fluorescence imaging (Fig. 2b), whereas microbots successfully delivered the 200-nm particles inside the KB cells when incubated for 3 h (Fig. 2c). The nanoparticles were found in subcellular vesicle compartments and were also free in the cytosol. The yellow co-localization signal in the images (Fig. 2c) was due to red-labelled cellular membranes and green nanoparticles. Optical confocal slices proved that green fluorescent-labelled particles were indeed inside the cells and not on the cell surface (Fig. 2d) and approximately twenty 200-nm particles (on average) entered the cells when transported with the microbots (Fig. 2e).

Detailed flow cytometry analysis was also performed with partial cell lysis and secondary antibody immunostaining to prove and characterize the uptake of the nanoparticles mediated by the bacteria (Fig. 3a−d). As expected, the secondary anti-mouse antibody did not enter the cells to stain the monoclonal antibody C11E9 that was delivered into the cells by means of microbots (Fig. 3a) until the cells were lysed by a mild detergent treatment. The cells (lower left quadrants in Fig. 3b,c) were incubated separately with streptavidin-coated 200-nm particles (upper left quadrants in Fig. 3b,c), *L. monocytogenes* only (lower right quadrants in Fig. 3b,c) and microbots with streptavidin-coated 200-nm particles (upper right quadrants in Fig. 3b,c). After removal of the non-cell-associated material, the samples were either left untreated (Fig. 3b) or lysed with Triton-X100 (Fig. 3c). Subsequently, all samples were stained with a phycoerythrin (PE)-conjugated monoclonal antibody against mouse IgG and were subjected to flow cytometry analysis using dual channels for fluorescein isothiocyanate (FITC) (FL1) and PE (FL4). An analysis

of the results of the PE readings (Fig. 3b,c) revealed that approximately 27% of the total PE signal (42%) was derived from intracellular sources, that is, from microbots (Fig. 3d). Approximately 15% of the total PE signal was either extracellular or cell membrane associated. Cells alone or KB cells with Listeria only samples did not have significant PE signals (Fig. 3d).

Microbots, docked with the model nucleic acid-based therapeutic GFP DNA, delivered the gene to the nucleus successfully, resulting in the expression of GFP as diffuse green fluorescence in the cytoplasm of KB cells (Fig. 4). Although the nanoparticles were intracellular at both 3 h (Fig. 4a) and 18 h (Fig. 4b) time points, the expression of GFP occurred at 18 h post-delivery (Fig. 4b,c). Dissociation of the nanoparticles from bacteria and the docked DNA from the nanoparticles may be facilitated by the low pH environment of the lysosomal compartments (Fig. 4d). Image analysis revealed a transfection efficiency of approximately $41.7 \pm 8.8\%$ (Fig. 4b,c; see also Supplementary Information, Fig. S5). The efficiency of bactofection has been reported to range from ∼2 to 20% (ref. 16). In three of the four tested cell lines (Caco2, COS-1, HeLa, HepG2), the efficiency was extrapolated to be less than 10% for the same study. We believe that the higher transfection efficiency using our approach is due to both nanoparticle properties (their high surface-to-volume ratio, which allows more cargo to be loaded) and the number of nanoparticles that can be docked onto the bacterial surface.

CYTOTOXICITY OF MICROBOTS

We examined the cellular cytotoxic response to 40-nm and 200-nm streptavidin-coated fluorescent polystyrene nanoparticles and to bacteria with nanoparticles in four cell lines from human solid-organ tumours (MCF-7, KB, HeLa, HepG-2). All cells rapidly responded to the nanoparticles within 1 h with acute lactate dehydrogenase (LDH) release, but their response gradually decreased (see Supplementary Information, Fig. S7). When compared with detergent-damaged positive control samples, all cells incubated with 40-nm particles alone showed up to 60% cytotoxicity within 1 h. Over three days this response gradually decreased to 14% and cells were dividing, indicating that they were metabolically active. Neither Listeria nor microbots with nanoparticles caused a drastic cellular cytotoxic response; the response was less than for the particles alone. These samples had less than approximately 20% of the cytotoxicity of the detergent-lysed cells, except for the *L. monocytogenes* sample with the HepG-2 cell line, which had a cytotoxic response of ∼40% (see Supplementary Information, Fig. S7b). Although the microbots had nanoparticles attached to them, the cells seemed to release more LDH for the nanoparticle-only samples. The 40-nm particles had higher cytotoxicity than the 200-nm particles because they can be taken up by the cells freely whereas the 200-nm particles are internalized only with the aid of microbots (Fig. 2). Invasion assays were also performed (see Supplementary Information, Fig. S7c) to evaluate the invasion efficiency of *L. monocytogenes*, *L. innocua* and the microbots for the four cell lines used in the study. The highest invasion was seen for the HepG-2 cells with *L. monocytogenes*.

GENE DELIVERY AND PROTEIN EXPRESSION IN MICE

Mice were injected intraperitoneally with microbots carrying the firefly luciferase gene on the 40-nm particle surface. Whole animal bioluminescence images (Fig. 5) showed that 3 days after infection, microbots successfully delivered the gene into the mice organs. The luciferase plasmid DNA was able to enter
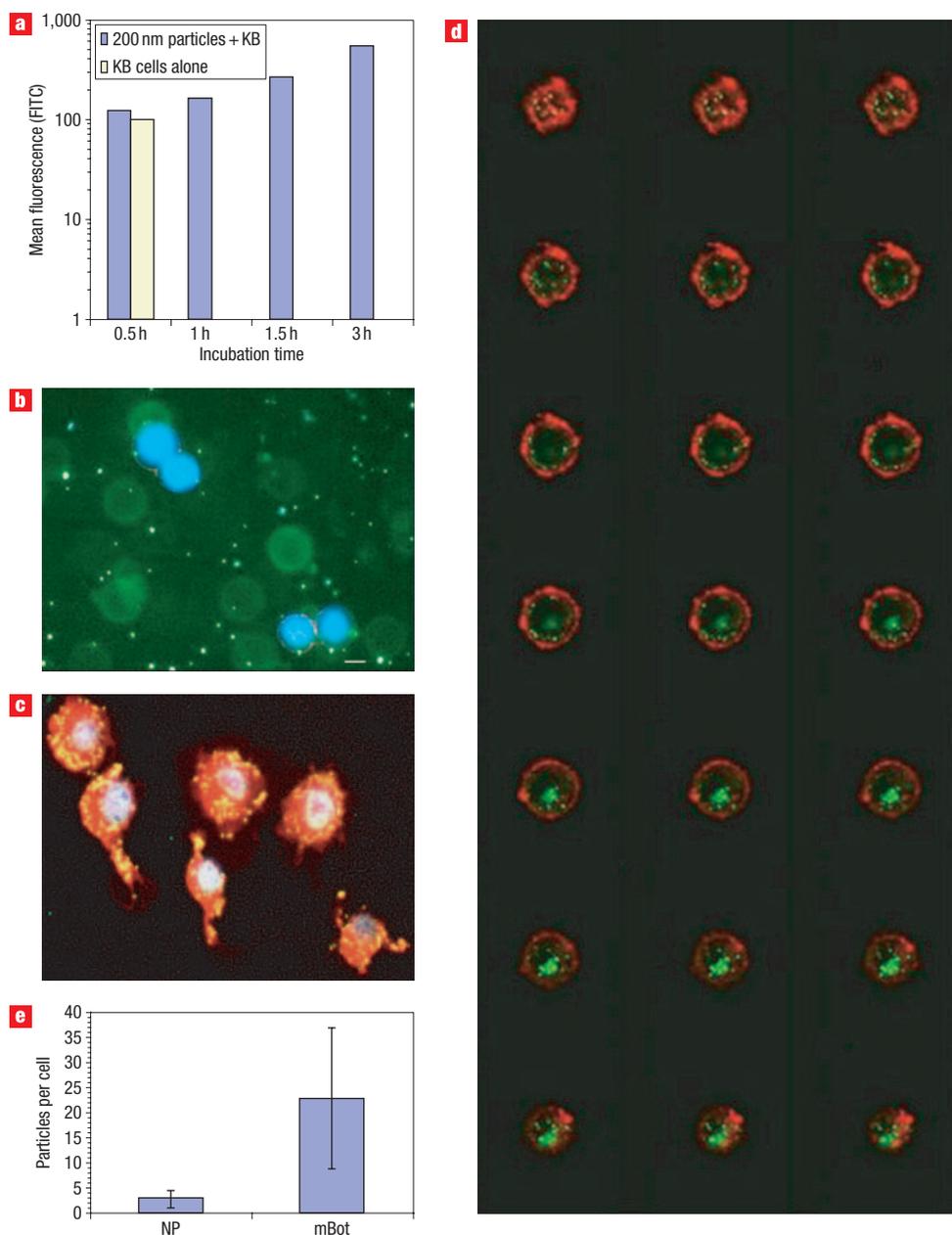
Figure 2 Internalization of microbots and their cargos. a, Time-dependent nonspecific association of 200-nm particles alone with KB cells. **b,c**, Fluorescence microscope images of cells incubated for 3 h with **b**, 200-nm particles alone (scale bar = 10 μm) and **c**, with microbots. **d**, Confocal microscope sections of a cell treated as in **c**, showing internalization. **e**, Average number of internalized nanoparticles per cell as calculated from panels **b−d** (NP, nanoparticle alone; mBot, with microbots). Cell membranes are red, nuclei are blue and nanoparticles are green in **b−d**. Yellow indicates internalization in **c**. Error bars represent standard deviations.

the nucleus and express the luciferase protein in the animals (Fig. 5a). There was no significant detectable endogenous luciferase activity in the animals injected with PBS as a control at 3 days post-injection (mean value 5 a.u., s.d. = 9.4, $n = 4$). Although all microbot-treated mice expressed the luciferase gene at a level of ∼380-fold ($3.81 \times 10^4\%$) more than the controls, the level of expression was highly variable in each animal (mean value 1,908 a.u., s.d. = 1,451, $n = 3$), as indicated by the photon counts per square pixel area of the expression regions from Fig. 5a (see also Fig. 5b). We were also able to elucidate the location of the fluorescent nanoparticles using a fluorescence illumination and background elimination setup (described in the Supplementary Information, Methods), which enabled us to co-localize nanoparticle locations (Fig. 6a) and luciferase expression. The luciferase activity was seen throughout the internal organs, but seemed to localize in kidney, liver/pancreas, intestine, spleen, pericardium and lungs (in order of decreasing signal strength; Figs 5a and 6b−d). As is clearly evident in Fig. 6, the majority of the luciferase expression was localized in an area including the liver, pancreas, duodenum, spleen and kidneys. The kidneys had unambiguously high luciferase activity.
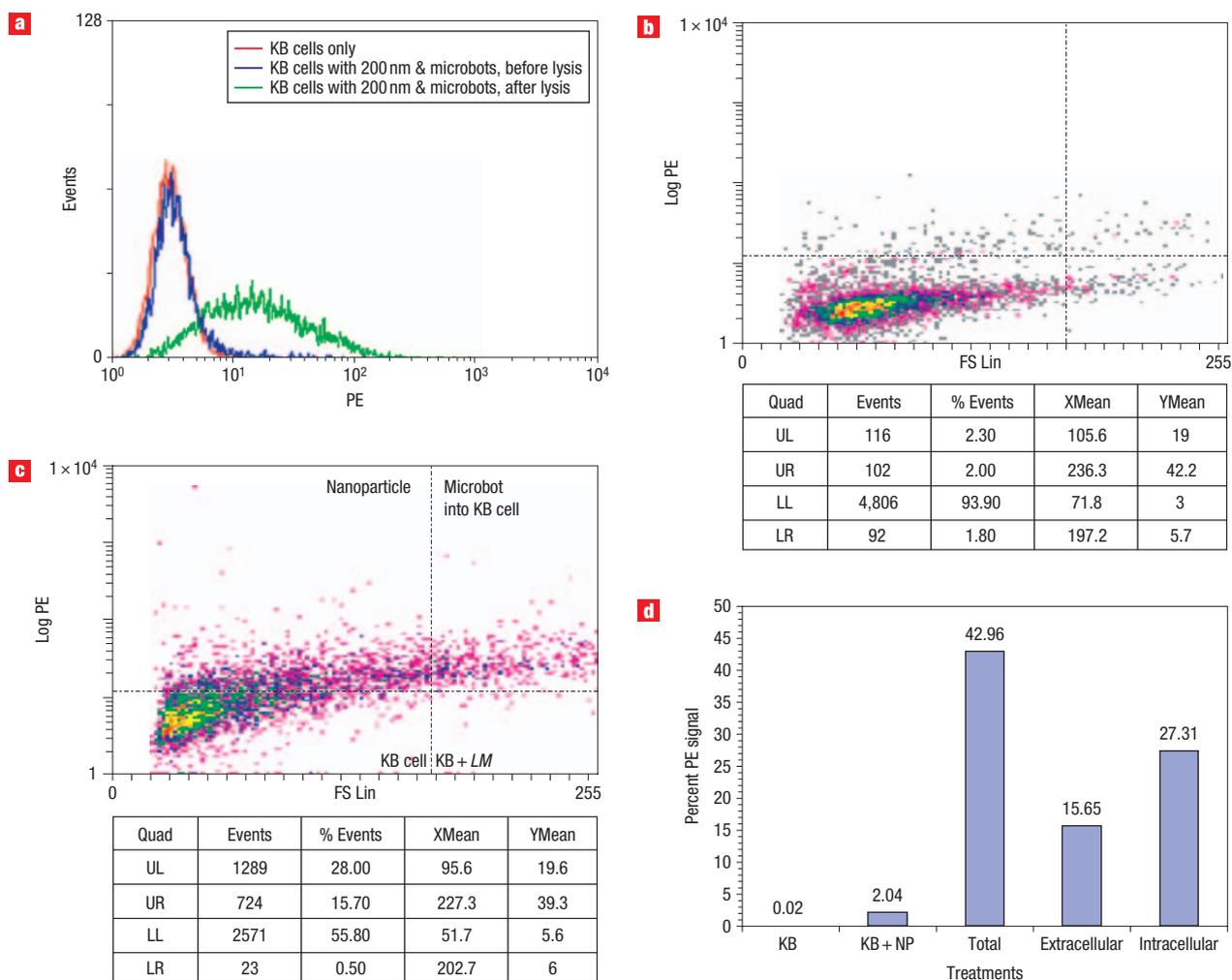
Figure 3 Flow-cytometric assessment of microbot uptake by cells. a, Evaluating the delivery of 200-nm particles into KB cells (red line) by flow cytometry. Treated cells were stained with phycoerythrin (PE)-labelled anti-mouse IgG antibodies before (blue line) and after (green line) cell lysis. Quantifying the internalization of **b**, nanoparticles alone and **c**, microbots. Quadrants in **b** and **c**: lower left (LL), KB cells; upper left (UL), 200-nm particles; lower right (LR), *L. monocytogenes* (*LM*) alone; upper right (UR), microbots with 200-nm particles; **d**, Evaluating the location of nanoparticles (NPs) with and without microbots. PE-labelled secondary antibody can access the interior of the cells only after cell lysis.

An alternative enzymatic method further verified the bioluminescence findings and quantified the microbot-mediated delivery and expression of the genes. Mice were injected with microbots carrying luciferase and SEAP gene cargoes and negative PBS-only controls. Three days later, select organs (liver, kidneys, spleen and intestines) were collected aseptically, enzymatically digested into homogenates and the expression of the reporter genes were quantified luminometrically (for luciferase) and chemiluminometrically (for SEAP). The luciferase assay had a signal half-life of 30 min, and, in preliminary assays, less than 5% signal intensity decay was observed within the reading time frame of the assays. In the luciferase and SEAP detection assay systems used, reporters yield linear assays with attomole sensitivities and no endogenous activity is associated with these reporters. Some intrinsic alkaline phosphatase activity can be found in various organs, but, being heat-labile, this enzyme is inactivated by treatment at 65 °C for 30 min, as was done here. Both luciferase (Fig. 6d) and SEAP (Fig. 6e) cargo molecules were delivered to the internal organs of live mice. Expressions of both reporter genes were highest in the intestinal

tissue, which is also a natural target organ for *L. monocytogenes*. Kidney and liver samples from microbot-treated mice had noticeable amounts of luciferase and SEAP protein activity. Although not tested, the bioluminescence images showed noticeable levels of luciferase activity in the gall bladder, lungs and heart as well. Luciferase expression levels in the homogenates of the tested organs were highly variable, evident from the large standard deviations in the luciferase enzymatic activity (Fig. 6d). This could be due to variability in the efficiency of the SV40 promoter driving the luciferase gene in different tissues. The level of SEAP enzyme activity was more uniform in the tested organs (Fig. 6e). *L. monocytogenes*, injected via the intraperitoneal route can disseminate into the internal organs of mice, with a majority of the bacteria are found in the liver, spleen, kidneys, peripheral blood mononuclear cells and central nervous system[30,31]. In line with these previous reports, in our study, the bioluminescence due to luciferase activity was also localized in the liver, pancreas, duodenum, spleen and kidneys. Some activity in the intestine, lungs and heart was also seen at lower levels of intensity, a finding that has also been reported
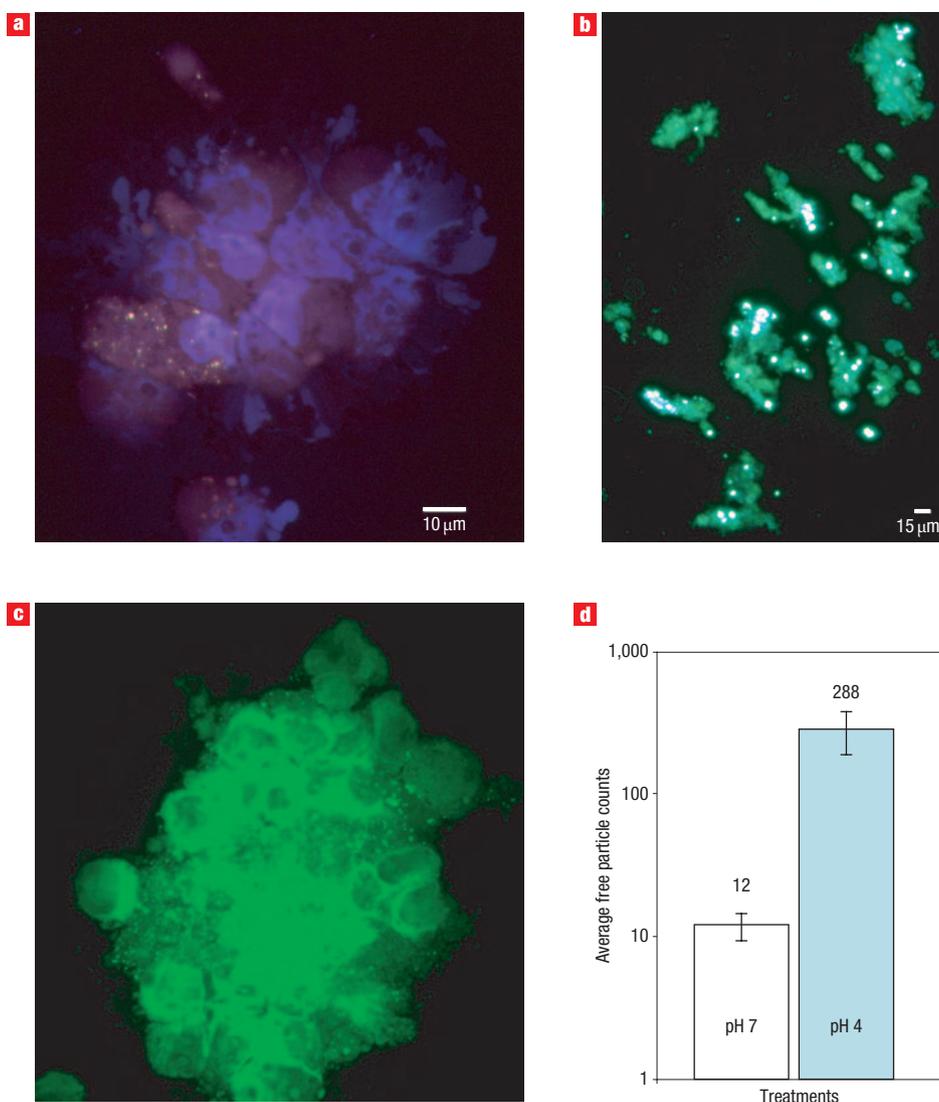
Figure 4 Intracellular delivery and expression of a model gene by microbots. a, Delivery of a plasmid DNA (coding for GFP) into KB cells using microbots at 3 h post-incubation. The cell membranes are red, nuclei are stained blue, and yellow indicates intracellular co-localization due to red (cells) and green (200-nm particles) signal overlap. **b**, A fluorescent micrograph (blue and green channels) of the sample in **a** at 18 h post-incubation. **c**, Expression of GFP from microbot-delivered DNA at a higher magnification ($\times 1,000$) at 18 h post-incubation. **d**, Disassociation of nanoparticles from the microbot surface at pH 4 and 7. Error bars represent standard deviations.

by others[32]. Signals seen around the lower thorax of the animals originate from the gall bladder, and this also has been well documented previously[32].

EFFICIENCY OF MICROBOT LOADING AND DELIVERY

From the confocal imaging studies, we found that each cell had approximately 22 200-nm particles (see Supplementary Information, Fig. S6). Because each microbot was carrying 1–3 particles, each human cell line used would therefore have at least 7–22 microbots. Previous immuno-electron microscopic analysis revealed a uniform distribution of C11E9 on the surface of *L. monocytogenes* cells, and the average number of C11E9-reactive antigens was approximately 190 per bacterium[25]; hence, it is reasonable to expect that a similar number of nanoparticles could be docked on each bacterial cell surface. The SEM images of the microbots (Fig. 1k) show that there are many

40-nm nanoparticles on the bacterial cell surface, supporting the previous findings that the cell surface receptors (N-acetylmuramidase) for antibody-C11E9 were uniformly distributed. This finding may also explain why microbots were fluorescing red in confocal and fluorescent microscopic images. The observed fewer numbers of 200-nm particles docked onto the bacterial cell surface may be due to steric hindrance, diffusion limitations or other physical barriers that preclude access or docking of 200-nm particles on the bacteria. Each 40-nm particle has a biotin-binding capacity of ~ 100, but for each 200-nm particle this value is 2×10^4 (from the certificate of analysis sheets of their manufacturer). Hence, each microbot is expected to carry biotinylated-DNA molecules in this range into target cells. The final spatial and temporal distribution of the microbots *in vivo* is determined by the invasion ability of *L. monocytogenes* for different tissue types and also by the filtration and sequestration of microbots or nanoparticles from the blood
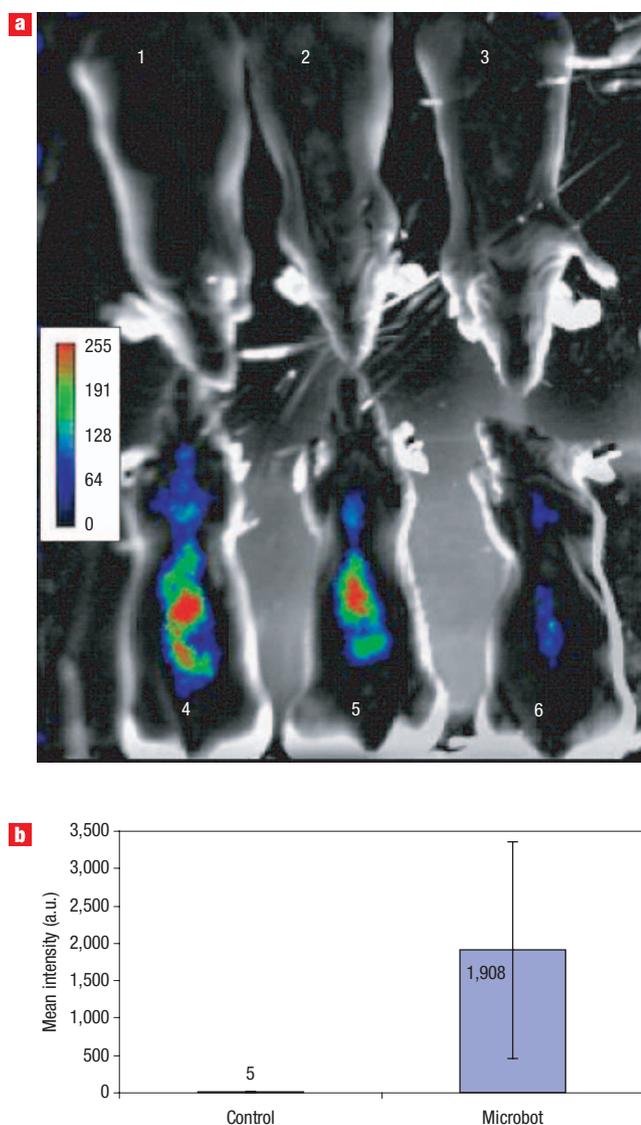
Figure 5 Microbot-mediated delivery and functional expression of luciferase gene in mice. a, In mice whole-animal bioluminescence images of mice with microbots carrying the firefly luciferase gene at three days post microbot treatment. Note the significant increase in photons collected from the microbot-treated animals (4–6) compared with the PBS-treated (sham-control) animals (1–3). The mice are in the ventro-dorsal position. **b**, Quantification of bioluminescence in sham-treated (white bar) and microbot-treated (blue bar) mice from **a**. On average, an ~380-fold increase in bioluminescence was observed in microbot-treated animals compared with PBS-treated mice ($n = 3$ animals per group, $P < 0.01$). Error bars represent standard deviations.

and lymphatic circulation system by different organs, in varying degrees.

DISCUSSION

In this study, we have demonstrated the bacteria-mediated delivery and visualization of different sized nanoparticles loaded with functional nucleic acid molecules into non-phagocytic mammalian cells of human solid organ tumours, and the successful expression of the cargo plasmid DNA (GFP) from the delivered nanoparticles. Liposomal or other encapsulated delivery methods suffer from the problem of entrapment in the subcellular vesicles and the biomolecule's inability to access the cytosol or other intended target sites such as the nucleus[33–36]. It is well known that *L. monocytogenes* can escape from the intracellular vesicles by means of the pore-forming activity of listeriolysin O. During this process the therapeutic molecules can diffuse into the cytoplasmic compartments. In a different approach reported earlier, *L. monocytogenes* was used to deliver DNA into the cytosol of mammalian cells by phage lysine mediated partial self-destruction of the carrier bacteria and by enhanced bacterial lysis due to the release of the intrinsically synthesized phage lysine[16].

Unlike these previously reported techniques, our approach is simple and versatile. Nanoparticles can be acquired commercially from various vendors, and have different surface functionalities, and different material and optical properties. Anchorage of the nanoparticles on the bacterial surface can easily be achieved using biotinylated antibodies, which serve as docking molecules through a streptavidin linkage. The 'nanovehicles' are linked to the bacteria by means of an antigen–antibody interaction, and the cargo and the bacteria can readily separate in the lower pH environment of the subcellular compartments, as made evident by the control experiments (Fig. 4d). Other factors, such as intracellular enzymatic processing or destabilization of antigen–antibody binding or a reduction in the biotin–streptavidin interactions can also be involved in the release mechanisms of the DNA, and all of these possibilities can potentially be used for endowing microbots with smart cargo release ability. Also, the use of intracellular bacteria in general and Listeria in particular for the delivery of nanoscale therapeutics has many advantages. Listeria bacteria have been shown to penetrate and colonize solid organ tumours[19,37] to which drugs circulating in the bloodstream have limited accessibility. Other nanoparticle-only based drug delivery approaches[38] still require the nanoparticles to be brought close to the tumour site, which is especially problematic in solid organ tumours and regions lacking vascularization.

In conclusion, microbots successfully delivered their cargos of nucleic acid-based model drugs, plasmid DNAs for firefly luciferase and SEAP enzymes into multiple organs of live mice, and the delivered genes also resulted in functional protein expression by three days post-treatment. As we have seen in the *in vitro* GFP expression assays, the delivered plasmid DNAs were able to escape from intracellular entrapment and were targeted to the nuclei of the cells, resulting in transcription and expression of the enzymes. Hence, this novel technology can be used to deliver these reporter molecules for whole-animal live imaging agents (luciferase) or for non-invasive *in vivo* reporter assays (SEAP). Our future studies will concentrate on the development of an attenuated Listeria strain, microbot-mediated delivery of artificial biohybrid nanostructures, delivery of larger size particles and functional proteins, and investigation of solid organ tumour penetration by microbots for applications in diagnostics and therapy at the single cell level and up to a few cells. Our bacteria-mediated nanoparticle and cargo delivery approach, which we term microbotics, promises excellent potential for nonviral gene delivery, and unique capabilities for biomedical nanorobotics and nanomedical therapy.

METHODS

PREPARATION OF MICROBOTS

Bacteria (10^8 colony forming units (c.f.u.) per ml, 1 ml) were incubated with a biotinylated monoclonal antibody C11E9[24–26] ($1 \mu g ml^{-1}$) at 22 °C for 30 min.
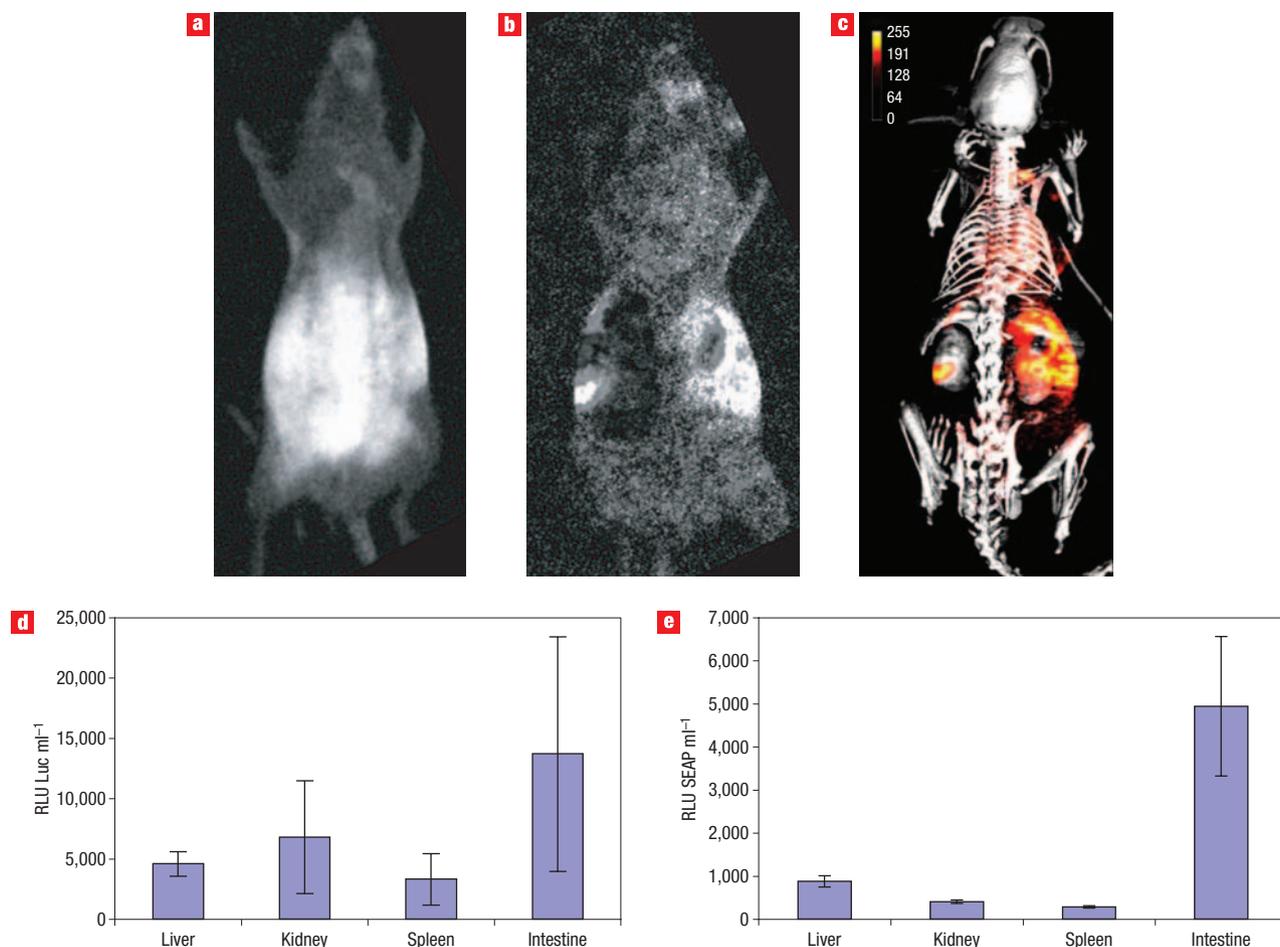
Figure 6 Characterization of *in vivo* protein expression. a, Live animal image of a mouse with microbots carrying the luciferase gene at three days post-injection. Locations of the nanoparticles were assessed by imaging (480 nm excitation, 523 nm band-pass emission-filter and 5 min exposure). **b**, A bioluminescence image of **a** with 35 min photon collection and integration. **c**, Anatomical localization of bioluminescence. A pseudo-coloured image of **b** was superimposed on a graphical anatomical image of a mouse to illustrate anatomical localizations of the signals. Mice are positioned ventro-dorsal in **a** and dorso-ventral in **b–c**. **d**, Enzymatic quantification of luciferase expression in organs of mice at three days post-injection. **e**, Enzymatic quantification of SEAP expression in organs of mice at three days post-injection (in relative light units, RLU). Error bars represent standard deviations.

After antibody attachment to the bacteria surface, two washes (see Supplementary Information) were performed to remove unreacted antibody. Streptavidin- or neutravidin-coated nanoparticles were then added (1×10^{10} ml^{-1}) and the mixture was incubated at room temperature for 15 min, at which time two low-speed washes were performed, and a centrifugal force of 3,000 g was applied for 5 min to preferentially spin down the bacteria, but not the nanoparticles. Microbots were diluted into PBS at 10^5 c.f.u. ml^{-1} and used immediately (or stored at 4 °C for no more than a week for SEM imaging studies). A biotinylated and rhodamine-labelled plasmid DNA vector encoding GFP under the control of a cytomegalovirus promoter (Gene Therapy Systems) was used as the model nucleic acid therapeutic molecule and was docked on the nanoparticle surfaces by streptavidin– or neutravidin–biotin interaction (see Supplementary Information, Methods, for details).

IMMUNOFLUORESCENCE ANALYSIS OF INTRACELLULAR AND EXTRACELLULAR MICROBOTS

After the initial infection process, cell monolayers were rinsed twice with PBS to remove unattached microbots and extra nanoparticles. Cells were trypsinized and recovered from the culture chambers, spun down at 300 g for 5 min and rinsed with Dulbecco's phosphate buffered saline (D-PBS) solution (Sigma) by performing a low-speed centrifugation as above. The cells were mounted on microscope slides and observed with a fluorescence microscope equipped with filters appropriate for FITC, Texas red and DAPI, and imaged using a cooled-colour CCD camera. Bacterial DNA was labelled with Hoechst-33342 stain for

15 min at room temperature. During some studies bacteria were also dual labelled with a lipophilic green-fluorescent cyanine-dye (DiO, Molecular Probes) and Hoechst stain.

FLOW CYTOMETRIC ASSESSMENT OF NANOPARTICLE UPTAKE

Tumour cells were grown in 24-well tissue culture plates to ~70% confluence and were rinsed with the fresh media. Either 40-nm or 200-nm nanoparticles were diluted in 10 μl of 1X Phosphate-Buffered Saline (PBS) to a final dilution of 0.01% (~10^9 particles) and were added to the wells of the tissue culture plate. The plates were returned back to the culture incubator and placed on a gently rotating stirrer for 0.5 h, 1 h, 2 h, 3 h and 3 days. To obtain cells in suspension, the cells were treated with 0.17% trypsin −0.02% EDTA (Sigma) at 37 °C for 1–3 min. Equal volumes of fresh medium were added to slow the digestion, and the cells were centrifuged at 300 g for 5 min. The supernatant was removed and the cells were washed once with wash buffer (PBS with 2% fetal bovine serum) as above. Finally, the cells were resuspended in the growth medium lacking serum and kept at 4 °C in an ice bath before being read in the flow cytometer. Each sample was assayed by flow cytometry (Epics XL, Coulter), and the data were analysed by both WinMDI and CellQuest software packages. To differentiate intracellular and extracellular microbots by fluorescence microscopy and flow cytometry, a dual-antibody staining procedure was used as described previously[39] and details are given in the Supplementary Information, Methods.

IN VIVO EXPRESSION STUDIES

Microbots were prepared as described above, except two different biotinylated plasmid DNAs coding for luciferase and SEAP were used instead of GFP[40]. The concentration of plasmid DNA per 100 μl of injection-ready microbot preparation was 5 μg DNA per 10^6 c.f.u. ml^{-1} of microbots, which were composed of 40-nm streptavidin-labelled Texas-red conjugated nanoparticles (10^{11} particles ml^{-1}) anchored on *L. monocytogenes* by means of monoclonal antibody C11E9. For analysis of *in vivo* delivery and expression, athymic (immunodeficient) nude mice (Nu$^-$Nu$^-$, all 5- to 6-week-old males, Harlan Sprague Dawley) were used throughout the studies as described in the Supplementary Information, Methods.

BIOLUMINESCENCE IMAGING

In vivo bioluminescence imaging was performed using a protocol detailed previously[20] using a Kodak Image Station and its acquisition and analysis software (Kodak). Additional image processing and quantifications were performed using ImageJ software (W. Rasband, National Institute of Health) as described in the Supplementary Information, Methods.

ENZYMATIC QUANTIFICATION ASSAYS FOR LUCIFERASE AND SEAP EXPRESSION

Organs (liver, kidneys, spleen and a small portion of the small intestine) from killed microbot-treated and untreated animals were collected aseptically into sterile plastic tubes and all subsequent sample processing was done on ice in these containers. All of the organs were homogenized separately in 200 μl reporter lysis buffer (Promega) on ice, centrifuged at 12,000 *g* for 1 min, and the supernatants were divided into two equal-sized aliquots and immediately used in the luciferase or SEAP assays, on the same day. For quantification of expression of luciferase, a kit-based assay in 96-well format (Promega) was used according to the instructions of the manufacturer of the kit.

ADDITIONAL METHODS

Additional details on the cell culture, invasion assays, nanoparticles, cytotoxicity assay, flow cytometry, confocal and bioluminescence imaging and analysis and enzymatic quantification of firefly luciferase and SEAP are available in the Supplementary Information.

References

1. Chan, W. C. & Nie, S. Quantum dot bioconjugates for ultrasensitive nonisotopic detection. *Science* **281,** 2016–2018 (1998).
2. Gao, X. *et al.* In vivo molecular and cellular imaging with quantum dots. *Curr. Opin. Biotech.* **16,** 63–72 (2005).
3. Lin, Z., Su, X., Mu, Y. & Jin, Q. Methods for labeling quantum dots to biomolecules. *J. Nanosci. Nanotech.* **4,** 641–645 (2004).
4. Voura, E. B., Jaiswal, J. K., Mattoussi, H. & Simon, S. M. Tracking metastatic tumor cell extravasation with quantum dot nanocrystals and fluorescence emission-scanning microscopy. *Nature Med.* **10,** 993–998 (2004).
5. Ballou, B., Ernst, L. A. & Waggoner, A. S. Fluorescence imaging of tumors in vivo. *Curr. Med. Chem.* **12,** 795–805 (2005).
6. West, J. L. & Halas, N. J. Engineered nanomaterials for biophotonics applications: improving sensing, imaging, and therapeutics. *Annu. Rev. Biomed. Eng.* **5,** 285–292 (2003).
7. Seppenwoolde, J. H. *et al.* Internal radiation therapy of liver tumors: qualitative and quantitative magnetic resonance imaging of the biodistribution of holmium-loaded microspheres in animal models. *Magn. Reson. Med.* **53,** 76–84 (2005).
8. Hattori, Y. & Maitani, Y. Enhanced in vitro DNA transfection efficiency by novel folate-linked nanoparticles in human prostate cancer and oral cancer. *J. Control. Release* **97,** 173–183 (2004).
9. Jain, R. K. Haemodynamic and transport barriers to the treatment of solid tumors. *Int. J. Radiat. Biol.* **60,** 85–100 (1991).
10. Maeda, H., Wu, J., Sawa, T., Matsumura, Y. & Hori, K. Tumor vascular permeability and the EPR effect in macromolecular therapeutics: a review. *J. Control. Rel.* **65,** 271–284 (2000).
11. Vassaux, G., Nitcheu, J., Jezzard, S. & Lemoine, N. R. Bacterial gene therapy strategies. *J. Pathol.* **208,** 290–298 (2006).
12. Vazquez-Boland, J. A. *et al.* Listeria pathogenesis and molecular virulence determinants. *Clin. Microbiol. Rev.* **14,** 584–640 (2001).
13. Finlay, B. B. & Cossart, P. Exploitation of mammalian host cell functions by bacterial pathogens. *Science* **276,** 718–725 (1997).
14. Vazquez-Boland, J. A., Dominguez-Bernal, G., Gonzalez-Zorn, B., Kreft, J. & Goebel, W. Pathogenicity islands and virulence evolution in *Listeria*. *Microbes Infect.* **3,** 571–584 (2001).
15. Hamon, M. L., Bierne, H. & Cossart, P. *Listeria monocytogenes*: a multifaceted model. *Nature Rev. Microbiol.* **4,** 423–434 (2006).
16. Pilgrim, S. *et al.* Bactofection of mammalian cells by *Listeria monocytogenes*: improvement and mechanism of DNA delivery. *Gene Ther.* **10,** 2036–2045 (2003).
17. Dietrich, G. *et al.* Delivery of antigen encoding plasmid DNA into the cytosol of macrophages by attenuated suicide *Listeria monocytogenes*. *Nature Biotechnol.* **16,** 862–866 (1998).
18. Sizemore, D. R., Branstrom, A. A. & Sadoff, J. C. Attenuated Shigella as a DNA delivery vehicle for DNA-mediated immunization. *Science* **270,** 299–302 (1995).
19. Darji, A. *et al.* Oral somatic transgene vaccination using attenuated *S. typhimurium*. *Cell* **91,** 765–775 (1997).
20. Paglia, P., Medina, E., Arioli, I., Guzman, C. A. & Colombo, M. P. Gene transfer in dendritic cells, induced by oral DNA vaccination with *Salmonella typhimurium*, results in protective immunity against a murine fibrosarcoma. *Blood* **92,** 3172–3176 (1998).
21. Yu, Y. A. *et al.* Visualization of tumors and metastases in live animals with bacteria and vaccinia virus encoding light-emitting proteins. *Nature Biotechnol.* **22,** 313–320 (2004).
22. Bermudes, D., Zheng, L. M. & King, I. C. Live bacteria as anticancer agents and tumor-selective protein delivery vectors. *Curr. Opin. Drug Discov. Devel.* **5,** 194–199 (2002).
23. Loeffler, D. I., Schoen, C. U., Goebel, W. & Pilgrim, S. Comparison of different live vaccine strategies in vivo for delivery of protein antigen or antigen-encoding DNA and mRNA by virulence-attenuated *Listeria monocytogenes*. *Infect. Immun.* **74,** 3946–3957 (2006).
24. Souders, N. C., Verch, T. & Paterson, Y. In vivo bactofection: Listeria can function as a DNA-cancer vaccine. *DNA & Cell Biol.* **25,** 142–151 (2006).
25. Souders, N. C., Sewell, D. A., Pan, Z. K., Hussain, S. F., Rodriguez, A., Wallecha, A. & Paterson, Y. Listeria-based vaccines can overcome tolerance by expanding low avidity CD8+ T cells capable of eradicating a solid tumor in a transgenic mouse model of cancer. *Cancer Immun.* **7,** 2–12 (2007).
26. Weber, W. & Fussenegger, M. Inducible gene expression in mammalian cells and mice. *Methods Mol. Biol.* **267,** 451–466 (2004).
27. Bhunia, A. K *et al.* Development and characterization of a monoclonal antibody specific for *Listeria monocytogenes* and *Listeria innocua*. *Infect. Immun.* **59,** 3176–3184 (1991).
28. Geng, T. *et al.* Expression of cellular antigens of *Listeria monocytogenes* that react with monoclonal antibodies C11E9 and EM-7G1 under acid-, salt- or temperature-induced stress environments. *J. Appl. Microbiol.* **95,** 762–772 (2003).
29. Geng, T., Hahm, B. K. & Bhunia, A. K. Selective enrichment media affect the antibody-based detection of stress-exposed *Listeria monocytogenes* due to differential expression of antibody-reactive antigens identified by protein sequencing. *J. Food Prot.* **69,** 1879–1886 (2006).
30. Drevets, D.A. Dissemination of *Listeria monocytogenes* by infected phagocytes. *Infect. Immun.* **67,** 3512–3517 (1999).
31. Bron, P. A., Monk, I. R., Corr, S. C., Hill, C. & Gahan, C. G. Novel luciferase reporter system for in vitro and organ-specific monitoring of differential gene expression in *Listeria monocytogenes*. *Appl. Environ. Microbiol.* **72,** 2876–2884 (2006).
32. Hardy, J., Margolis, J. J. & Contag, C. H. Induced biliary excretion of *Listeria monocytogenes*. *Infect Immun.* **74,** 1819–1827 (2006).
33. Miller, A. D. The problem with cationic liposome/micelle-based non-viral vector systems for gene therapy. *Curr. Med. Chem.* **10,** 1195–2110 (2003).
34. El-Aneed, A. An overview of current delivery systems in cancer gene therapy. *J. Control. Rel.* **94,** 1–14 (2004).
35. Lechardeur, D. & Lukacs, G. L. Intracellular barriers to non-viral gene transfer. *Curr. Gene Ther.* **2,** 183–194 (2002).
36. Cheong, I. *et al.* A bacterial protein enhances the release and efficacy of liposomal cancer drugs. *Science* **314,** 1308–1311 (2006).
37. Michl, P. and Gress, T. M. Bacteria and bacterial toxins as therapeutic agents for solid tumors. *Curr. Cancer Drug Targets.* **4,** 689–702 (2004).
38. Braun, L., Nato, F., Payrastre, B., Mazie, J. C. & Cossart, P. The 213-amino-acid leucine-rich repeat region of the *Listeria monocytogenes* InlB protein is sufficient for entry into mammalian cells, stimulation of PI 3-kinase and membrane ruffling. *Mol. Microbiol.* **34,** 10–23 (1999).
39. Tang, P., Foubister, V., Pucciarelli, G. & Finlay, B. B. Methods to study bacterial invasion. *J. Microbiol. Methods* **18,** 227–240 (1993).
40. Zreiqat, H., Sungaran, R., Howlett, C. R. & Markovic, B. Quantitative aspects of an in situ hybridization procedure for detecting mRNAs in cells using 96-well microplates. *Mol. Biotechnol.* **10,** 107–113 (1998).

Author contributions

D.A. and R.B. designed the experiments. D.A. performed and was involved in all aspects of the experiments; J.S. performed confocal and fluorescence imaging; K.R. and J.P.R. performed the flow cytometry; and D.S. performed the SEM imaging. D.A., K.B. and A.B. designed and performed the cytotoxicity studies. S.M. assisted in *in vivo* studies. D.A. and R.B. co-wrote the paper.